Pergamon

Int. J. Heat Mass Transfer. Vol. 38, No. 6, pp. 1097–1104, 1995

0017-9310/95 $9.50 + 0.00

0017-9310(94)00226-6

The natural convection from a point heat source embedded in a non-Darcian porous medium

JIN-SHENG LEU and JIIN-YUH JANG†

Department of Mechanical Engineering, National Cheng-Kung University, Tainan, Taiwan 70101, Republic of China

(*Received* 24 *December* 1993 *and in final form* 27 *June* 1994)

Abstract—The natural convection flow from a heat point source embedded in a non-Darcian porous medium is investigated by employing local similarity and modified Keller's Box methods. The non-Darcian effects of convective, inertia and thermal dispersion are all considered. The results indicate that the non-Darcian effects decrease the centerline velocity and temperature and also increase the velocity and temperature boundary layer thicknesses. In addition, solutions using the local similarity method overestimate the centerline velocity and temperature.

INTRODUCTION

The steady buoyancy-induced flow arising from thermal energy sources is commonly referred to as a natural convection plume. Among such plumes, two general types may be identified—the free plume and the wall plume. The free plume is typified by the buoyant flow above a heated sphere or a horizontal cylinder. A typical wall plume is the flow resulting from a heat source along the base of an adiabatic vertical plate. The free and wall plumes from a line or a point thermal source in a viscous fluid have been studied extensively (see, for example, refs. [1–5], and the references cited therein). However, the analogous problems of free and wall plumes in a saturated porous medium have received rather less attention. The applications include the natural convection cooling of buried electrical cables, the disposal of nuclear wastes, hot-wire anemometry, volcanic eruption, etc.

Wooding [6] developed a boundary-layer theory for steady-state natural convection from a line or point source in an infinite Darcian saturated porous medium. In what follows, Bejan [7] carried out in some detail the boundary layer analysis for the plume above a point source in a porous medium. Lai [8] re-examined the same problem for a point source, using a more suitable similarity variable, and he also obtained a closed form solution. Bejan [9] used a perturbation analysis to study the transient and steady natural convection from a point heat source at low Rayleigh number in a Darcian porous medium of infinite extent. The steady point heat sources at low and high Rayleigh numbers in an unbounded Darcian porous medium were investigated by Hickox and Watts [10] and Hickox [11]. Afzal and Salam [12] studied the natural convection arising from a point source in a Darcian porous medium bounded by an adiabatic conical surface. Nakayama [13] solved the boundary layer equations for free convection from a point heat source in a Darcian porous medium saturated with a non-Newtonian power-law fluid. The Darcian mixed convection from a line thermal source imbedded at the leading edge of an adiabatic vertical surface in a saturated porous medium was numerically analyzed by Kumari *et al.* [14].

Coupled heat and mass transfer by natural convection at low Rayleigh number in an infinite Darcian porous medium has been reported by Poulikakos [15] for a point source, by Larson and Poulikakos [16] for a line source and by Lai and Kulacki [17] for a sphere. For a large Rayleigh number, Lai [18] obtained the similarity solution for a line source, and the closed form solutions are presented for the special case of Lewis number equal to 1.

All of the works mentioned above are based on the Darcy formulation. However, at a high Rayleigh number or in a high porosity medium, there is a departure from Darcy's law and the convective, boundary friction (no-slip), inertia and thermal dispersion effects not included in the Darcy model may become significant. Ingham [19] obtained an exact solution for the free convection from a line source in an unbounded non-Darcian porous medium when only the inertia effect is considered, and he shows that the non-Darcian flow would produce a much more peaked temperature profile than that predicted by the Darcian flow. Local non-similarity solutions are reported by Lai [20] for natural convection from a line source to examine the inertia and thermal dispersion effects. It is found that the inertial effect tends to reduce the flow and temperature profile while thermal dispersion effect enhances this influence further. Cheng and Zheng [21] used the local similarity method to study the mixed convection plume above a hori-

†Author to whom correspondence should be addressed.

NOMENCLATURE

C	inertia coefficient	α_0	stagnant thermal diffusivity
C_p	specific heat of fluid	β	coefficient of thermal expansion
Da_x	Darcy number, K/x^2	Γ	dimensionless inertia parameter, $K^2C^2g\beta Q/2\pi k\alpha_0 v$
d	mean particle diameter		
f	dimensionless stream function	γ	thermal dispersion coefficient
g	gravitational acceleration	ε	porosity
k	effective conductivity	ξ	parameter, $1/Da_x\, Ra_x^{1/2} = (2\pi k\alpha_0 vx^2/g\beta QK^2)^{1/2}$
K	permeability		
Pr	Prandtl number, v/α_0	η	pseudo-similarity variable, $r(Ra_x)^{1/4}/x$
Q	strength of thermal point source		
Ra_d	Rayleigh number based on the particle diameter, $g\beta Qd^2/2\pi k\alpha_0 v$	θ	dimensionless temperature, $2\pi kx(T-T_\infty)/Q$
Ra_x	local Rayleigh number, $g\beta Qx^2/2\pi k\alpha_0 v$	μ	fluid dynamic viscosity
T	temperature	v	fluid kinematic viscosity
u, v	volume averaged velocity in the x, r directions	ρ	fluid density
		ψ	stream function.
x, r	axial and radial coordinates.		

Greek symbols

α_d	thermal diffusivity due to thermal dispersion effect

Subscript

∞	condition at the free stream.

zontal line source. The inertia and thermal dispersion effects are included. It is noted that the numerical methods used in refs. [20, 21], such as the local similarity method and the local nonsimilarity method, have their own drawbacks, as the derivatives of certain terms are discarded in order to reduce the partial differential equations to ordinary differential equations. The rigorous numerical solutions for the natural convection flow from the free plume above a heat source in a non-Darcian porous medium (combined convective, inertia effects and thermal dispersion) does not seem to have been investigated. This has motivated the present investigation. It is noted that, in the absence of a bounding surface, the boundary friction effect does not exist in the present problem.

The object of the present analysis is to study the natural convection from the free plume due to a point heat source in a non-Darcian porous medium. The non-Darcian effects of convective, inertia and thermal dispersion are all considered. The governing partial differential equations are solved using a suitable variable transformation and employing an efficient finite-difference Keller's Box method [22], incorporated with a numerical algorithm developed by Yu *et al.* [23] to deal with the integral boundary condition. The non-Darcian effects on the temperature and velocity fields will be examined in detail. In addition, the local similarity solution is also presented in order to check the accuracy of this approximate method for the present problem.

MATHEMATICAL ANALYSIS

We consider the free convection from a point heat source, generating heat at rate Q, which is embedded in an unbounded porous medium. The physical model and coordinate system are illustrated in Fig. 1. In order to study transport through non-Darcian media, the original Darcy model is improved by including convective, inertia and thermal dispersion effects. In addition, if we assume that: (1) the convective fluid and porous medium are in local thermal equilibrium,

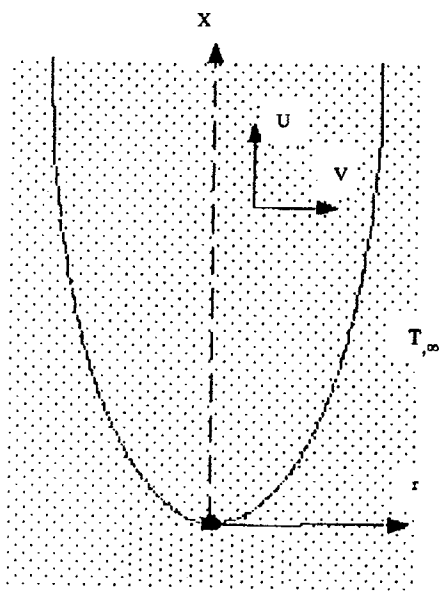

Fig. 1. The physical model and coordinate system.

(2) the properties of the fluid except for the density term that is associated with the body force are constant, and (3) the boundary layer approximations are employed, then the governing equations become

$$\frac{\partial(ru)}{\partial x}+\frac{\partial(rv)}{\partial r}=0 \tag{1}$$

$$\frac{\rho}{\varepsilon^2}\left(u\frac{\partial u}{\partial x}+v\frac{\partial u}{\partial r}\right)=\rho_\infty g\beta(T-T_\infty)-\frac{\mu}{K}u-\rho Cu^2 \tag{2}$$

$$u\frac{\partial T}{\partial x}+v\frac{\partial T}{\partial r}=\frac{1}{r}\frac{\partial}{\partial r}\left[r(\alpha_0+\alpha_d)\frac{\partial T}{\partial r}\right] \tag{3}$$

where x and r are the axial and radial coordinates, respectively; K is the permeability of the porous medium; C is the transport property related to the inertia effect; ε is porosity; α_0 is the stagnant thermal diffusivity and α_d is the molecular diffusivity due to transverse (radial) thermal dispersion. The other symbols are defined in the Nomenclature. Here we adopt the following thermal dispersion model proposed by Plumb [24], that is

$$\alpha_d=\gamma ud \tag{4}$$

where γ is the dispersion coefficient, which has a value ranging from 1/7 to 1/3 and d is the mean particle diameter.

The boundary conditions for equations (1)–(3) are

$$\begin{aligned} &x=0 \quad r>0 \quad u=0 \quad T=T_\infty\\ &x>0 \quad r=0 \quad \frac{\partial u}{\partial r}=0 \quad v=0 \quad \frac{\partial T}{\partial r}=0\\ &r\to\infty \quad T=T_\infty. \end{aligned} \tag{5}$$

According to the principle of conservation of energy, the conservation of energy requires that, at any position $x>0$, the convective energy is equal to the energy released by the point heat source, Q. Thus

$$Q=2\pi\rho_\infty C_p\int_0^\infty u(T-T_\infty)r\,dr. \tag{6}$$

We introduce the following transformations:

$$\begin{aligned} &\eta=\frac{r}{x}(Ra_x)^{1/4} \quad \xi(x)=\frac{1}{Da_x\,Ra_x^{1/2}}\\ &f(\xi,\eta)=\frac{\psi(x,r)}{\alpha_0 x} \quad \theta(\xi,\eta)=\frac{T(x,r)-T_\infty}{Q/2\pi kx} \end{aligned} \tag{7}$$

where $Ra_x=g\beta Qx^2/2\pi k\alpha_0 v$ is the local Rayleigh number; $Da_x=K/x^2$ is the local Darcy number and ψ is the Stokes stream function, which automatically satisfies the continuity equation (1). The parameter ξ characterizes the source strength (Q), the distance along the plate from the leading edge (x) and the permeability (K) of the porous medium. As x increases or Q, K decreases, the value of $\xi(x)$ increases.

Substituting equation (7) into equations (1)–(3), we obtain

$$\theta-\frac{1}{\varepsilon^2 Pr\,\eta^3}(ff'^2-\eta ff'')-\xi\frac{f'}{\eta}-\frac{\Gamma^{1/2}}{Pr}\xi\left(\frac{f'}{\eta}\right)^2=\frac{\xi}{\varepsilon^2 Pr\,\eta^3}\left[(f'-\eta f'')\frac{\partial f}{\partial\xi}+\eta f'\frac{\partial f'}{\partial\xi}\right] \tag{8}$$

$$\eta\theta''+\theta'+(f'\theta+f\theta')+\gamma\,Ra_d^{1/2}(f''\theta'+f'\theta'')=\xi\left(f'\frac{\partial\theta}{\partial\xi}-\theta'\frac{\partial f}{\partial\xi}\right) \tag{9}$$

where the primes denote partial differentiation with respect to η, $Pr=\nu/\alpha_0$ is the Prandtl number, $\Gamma=K^2C^2g\beta Q/2\pi k\nu\alpha_0$ is a dimensionless inertia parameter expressing the relative importance of the inertia effect; $Ra_d=g\beta Qd^2/2\pi k\alpha_0\nu$ is the Rayleigh number based on the particle diameter.

It is noted that Darcy's law corresponds to the case of $\xi\to\infty$ (i.e. $K\to 0$) with $\Gamma=0$ and $\gamma=0$, for which analytical solutions can be obtained [7]. For Darcy's law, the closed-form solutions in terms of the variables (ξ,η) of the present study are as follows:

$$f'=\frac{256\eta}{3\xi\left(\eta^2\xi^{-1}+\frac{32}{3}\right)^2} \tag{10}$$

$$\theta=\frac{256}{3\left(\eta^2\xi^{-1}+\frac{32}{3}\right)^2}. \tag{11}$$

The transformed boundary conditions for equations (8)–(9) are

$$f(\xi,0)=f'(\xi,0)=\theta'(\xi,0)=0 \quad \theta(\xi,\infty)=0 \tag{12}$$

and the constraint is

$$\int_0^\infty f'\theta\,d\eta=1. \tag{13}$$

In terms of new variables, it can be shown that the dimensional velocity components and temperature are given by

$$\begin{aligned} u&=\left(\frac{g\beta Q\alpha_0}{2\pi k\nu}\right)^{1/2}\frac{f'(\xi,\eta)}{\eta}\\ v&=\alpha_0 K^{-1/2}\xi^{-1/2}\left(\frac{1}{2}f'-\frac{f}{\eta}-\frac{\xi}{\eta}\frac{\partial f}{\partial\xi}\right)\\ T-T_\infty&=\left(\frac{Q\nu\alpha_0}{2\pi g\beta k}\right)^{1/2}\frac{\theta(\xi,\eta)}{K\xi}. \end{aligned} \tag{14}$$

NUMERICAL METHOD

In this study, both the local similarity and Keller's Box finite-difference methods were used. For the finite-difference method, equations (8) and (9) associated with boundary conditions (12) were solved by an efficient and accurate implicit finite-difference method similar to that described in Cebeci and Bradshaw [22].

To begin with, the partial differential equations are first converted into a system of first-order equations; then these first-order equations are expressed in finite-difference forms in terms of center difference. Denoting the mesh points in the ξ–η plane by ξ_i and η_j, where $i = 0, 1, \ldots, M$ and $j = 0, 1, \ldots, N$, this results in a set of nonlinear difference equations for the unknown at ξ_i in terms of their values at ξ_{i-1}. The resulting nonlinear finite-difference equations are then solved by Newton's iterative method. The boundary layer equations are thus solved step by step by taking the converged solution at $\xi = \xi_{i-1}$. To initiate the process, equations (8) and (9) with $\xi = 0$ are first solved by using a sixth-order variable-step-size Runge–Kutta integration scheme. After obtaining a converged solution along $\xi = 0$, this solution is then employed in a Keller Box scheme with second-order accuracy to march step by step along the boundary layer.

We adopted the numerical algorithm [23] to deal with the integral constraint equations (13). We first drop the boundary condition $\theta'(\xi,0) = 0$, and assume another presupposed boundary condition $\theta(\xi,0) = s$, where s is the undetermined nonzero constant. The refined value of s can be estimated by the Newton–Raphson method, associated with one set of variation equations which were derived by taking the derivatives of the finite-difference equations of equations (8) and (9) and their boundary condition (12) with respect to s. These variation equations can also be solved by using Keller's scheme (the details can be seen in ref. [22]). The dropped boundary condition, together with the integral condition, equation (13), are treated as constraints. The iterations for adjusting the presupposed boundary condition are repeated until the following criterion, which is the sum of squares of the discrepancies for the constrained conditions, is satisfied:

$$[\theta'(\xi,0)]^2 + \left[\int_0^\infty f'\theta \, d\eta - 1\right]^2 \leqslant \text{error (say, } 10^{-7}).$$

In the calculations, the values of $\eta_\infty = 20$ was found to be sufficiently accurate for $|\theta_\infty| < 10^{-3}$. Uniform step sizes of $\Delta\eta = 0.05$ in the η-direction and $\Delta\xi = 0.1$ in the ξ-direction were used.

For the local similarity method, this problem consists of solving only equations (8) and (9) when the right-hand sides of these equations are replaced by zero. A sixth-order variable-step-size Runge–Kutta integration routine in conjunction with the Newton–Raphson iterative scheme is used here to solve equations (8) and (9). The η_∞ decreased gradually with increasing ξ and ranged from $\eta_\infty = 20$ for $\xi = 0$ to $\eta_\infty = 5$ for $\xi = 8$.

RESULTS AND DISCUSSIONS

Three different solid–fluid combinations shown in Table 1 were used in this study. The values of permeability K and inertia coefficient C were calculated by employing the Ergun model [25]: $K = d^2\varepsilon^3/[150(1-\varepsilon)^2]$, $C = 1.75(1-\varepsilon)/\varepsilon^3 d$.

Figures 2 and 3 show the finite-difference solutions of the dimensionless tangential velocity

$$\frac{u}{(g\beta Q\alpha_0/2\pi k\nu)^{1/2}}\left(=\frac{f'}{\eta}\right)$$

and temperature

$$\frac{(T-T_\infty)}{(Q\nu\alpha_0/2\pi g\beta K^2 k)^{1/2}}\left(=\frac{\theta}{\xi}\right)$$

profiles across the boundary layer, respectively, at different values of ξ with $Pr = 5.4$, $\Gamma = 1200$ and with no thermal dispersion taken into consideration ($\gamma = 0$). The dashed lines denote the analytical solutions based on the Darcy model ($\xi = \infty$, $\Gamma = 0$ and $\gamma = 0$) [7]. The dimensionless abscissa is set to $\eta\xi^{0.5}$ ($= r/K^{1/2}$). It is seen that the centerline velocity and temperature decrease with increasing values of ξ; that is, both the centerline velocity and temperature decrease with the increasing downstream distance x for given source strength Q and permeability K, or decrease with the decreasing Q for fixed x and K. In addition, the temperature boundary layer thickness increases as ξ increases. It is also observed that Darcy's solutions overestimate the centerline velocity and temperature. It is also shown that, as may be expected, Darcy's law is only valid for large values of ξ.

Figures 4 and 5 show the finite-difference solutions of the inertia effect ($\Gamma = 1200$, 4800, 37 120) on the dimensionless tangential velocity and temperature profiles, respectively, at $\xi = 2$ with $\gamma = 0.15$ and $Ra_d = 300$. The dash lines represent the Darcy model [7]. It is seen that the inertia effects significantly flatten the velocity and temperature profiles and thicken the velocity and temperature boundary layer thicknesses. This is because the form drag of the porous medium is increased, when the inertia effect is included. The results also indicate that, as the value of Γ is increased, the centerline velocity is decreased, while the centerline temperature is increased. To visualize the inertia effect on the temperature fields, the dimensionless isotherms for $\theta/\xi = 0.25$ generated for $\Gamma = 1200$, 4800 and 37 120 with $\gamma = 0.15$ and $Ra_d = 300$ are plotted in Fig. 6. The dimensionless ordinate and abscissa variables are set to

$$\xi\left(=\frac{x}{(g\beta K^2 Q/2\pi k\nu\alpha_0)^{1/2}}\right)$$

and

$$\eta\xi^{0.5}\left(=\frac{r}{K^{1/2}}\right).$$

The dashed line represents the Darcy model. It is seen that the centerline temperature expands farther for a Darcy model and makes the isotherm of Darcy model more slender. This is due to the fact that the Darcy model overestimates the heat transfer rate; thus heat

Table 1. Three different solid–fluid combinations and heat source strength used in this study with $Pr = 5.4$

Fluid	Solid	d [mm]	ε	Q [W]	K [m^2]	C [m^{-1}]	Γ
Water	Glass	3	0.375	200	8×10^{-9}	6913	1200
Water	Glass	6	0.4	200	4×10^{-8}	2836	4800
Water	Glass	15	0.453	200	4.6×10^{-7}	686	37 120

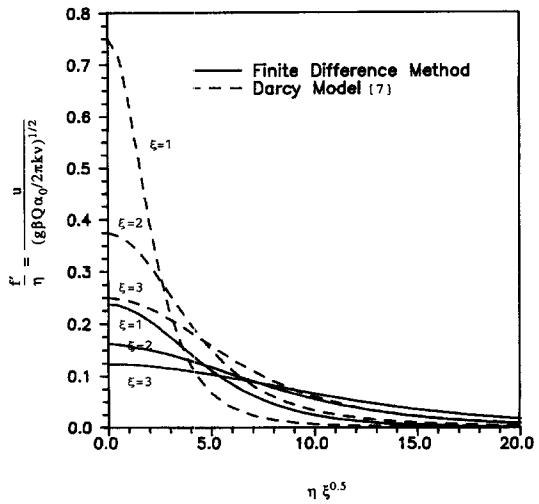

Fig. 2. The dimensionless tangential velocity profiles across the boundary layer at $\xi = 1$, 2 and 3 with $Pr = 5.4$, $\Gamma = 1200$ and $\gamma = 0$.

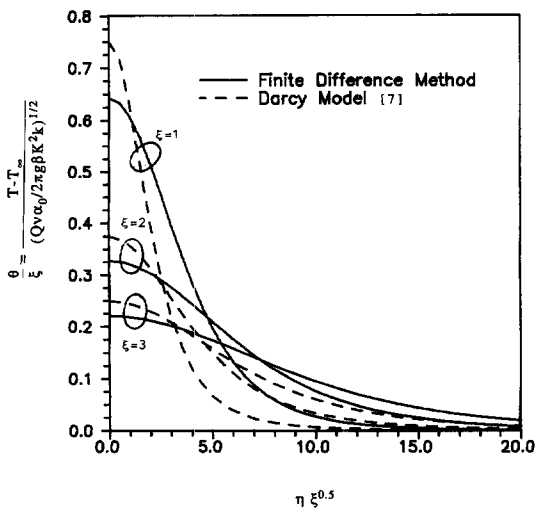

Fig. 3. The dimensionless temperature profiles across the boundary layer at $\xi = 1$, 2 and 3 with $Pr = 5.4$, $\Gamma = 1200$ and $\gamma = 0$.

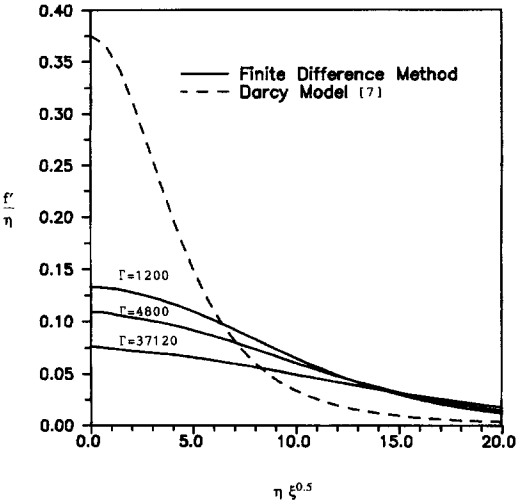

Fig. 4. The dimensionless tangential velocity profiles across the boundary layer for $\Gamma = 1200$, 4800 and 37 120 at $\xi = 2$ with $Pr = 5.4$, $\gamma = 0.15$ and $Ra_d = 300$.

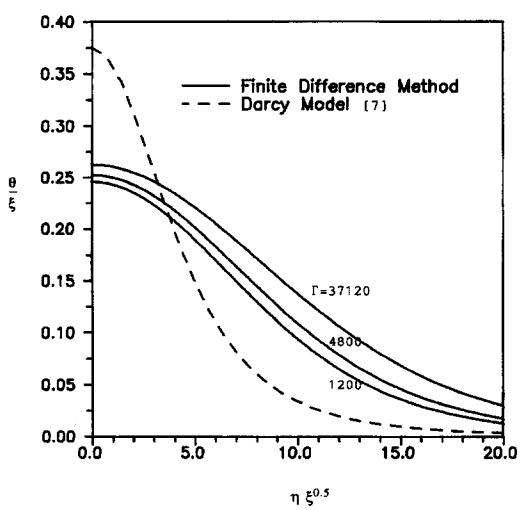

Fig. 5. The dimensionless temperature profiles across the boundary layer for $\Gamma = 1200$, 4800 and 37 120 at $\xi = 2$ with $Pr = 5.4$, $\gamma = 0.15$ and $Ra_d = 300$.

is more easily transferred in the downstream direction. Moreover, as Γ increases, the temperature boundary layer thickness is increased, therefore the isotherms become flatter.

Figures 7 and 8 show the finite-difference solutions of the thermal dispersion effect ($\gamma = 0$, 0.15, 0.3) on the dimensionless tangential velocity and temperature profiles, respectively, at $\xi = 1$ with $\Gamma = 1200$, $Ra_d = 300$. The dashed lines represent the Darcy model[7]. It is seen that, as the value of γ is increased, both the centerline velocity and temperature decrease. We also observe that the velocity and temperature boundary layer thicknesses increase with increasing values of γ. This is expected as the transverse (or

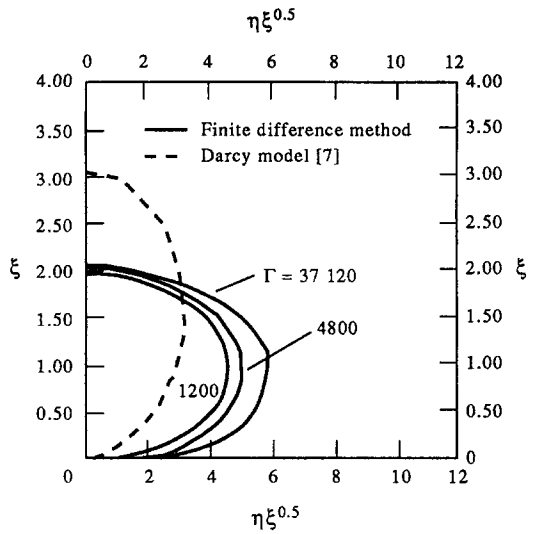

Fig. 6. The dimensionless isotherms for $\theta/\xi = 0.25$ generated for $\Gamma = 1200$, 4800 and 37 120 with $\gamma = 0.15$ and $Ra_d = 300$.

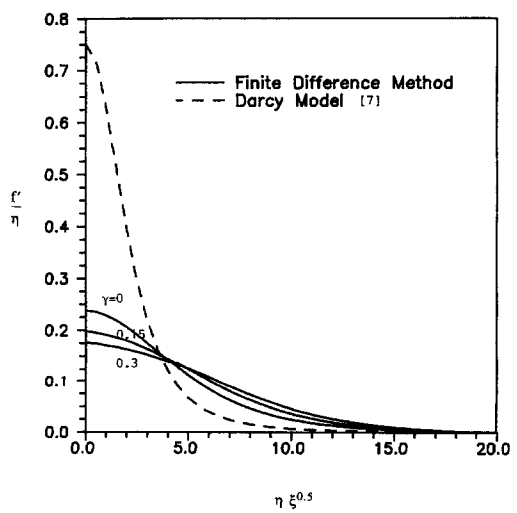

Fig. 7. The dimensionless tangential velocity profiles across the boundary layer for $\gamma = 0$, 0.15 and 0.3 at $\xi = 1$ with $Pr = 5.4$, $\Gamma = 1200$ and $Ra_d = 300$.

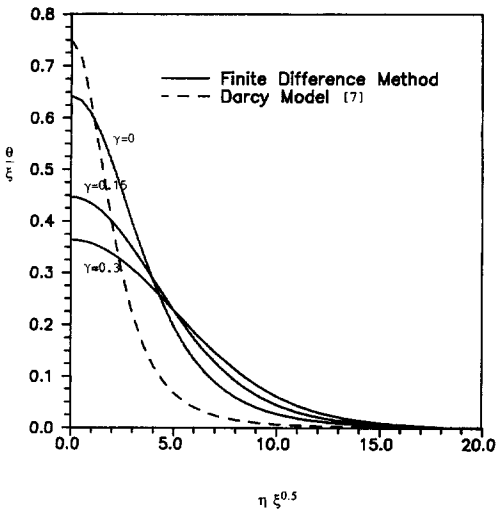

Fig. 8. The dimensionless temperature profiles across the boundary layer for $\gamma = 0$, 0.15 and 0.3 at $\xi = 1$ with $Pr = 5.4$, $\Gamma = 1200$ and $Ra_d = 300$.

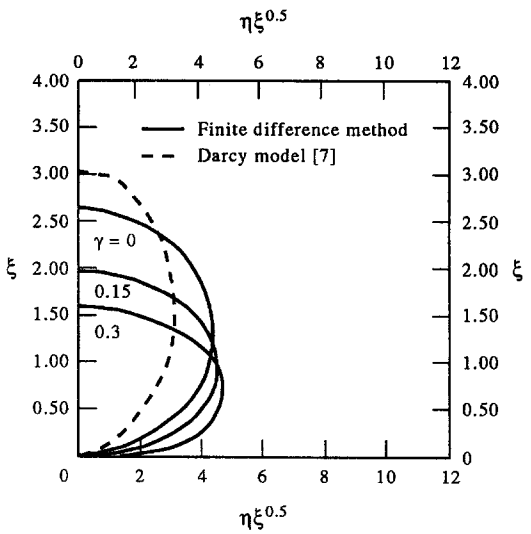

Fig. 9. The dimensionless isotherms for $\theta/\xi = 0.25$ generated for $\gamma = 0$, 0.15 and 0.3 with $\Gamma = 1200$ and $Ra_d = 300$.

radial) thermal dispersion effect increases the effective thermal conductivity of the packed bed. The dimensionless isotherms for $\theta/\xi = 0.25$ generated for $\gamma = 0$, 0.15 and 0.3 are shown in Fig. 9. The dashed line denotes the Darcy model. It is seen that, when the thermal dispersion effect is included, the isotherms become flatter. This is due to the fact that the value of effective thermal conductivity of the packed bed is increased, and thus heat is more easily transferred in the transverse direction.

The variations of the centerline temperature and velocity over a wide range of ξ are shown in Fig. 10(a) and (b), respectively, for $\Gamma = 1200$, $\gamma = 0.15$ and $Ra_d = 300$. The local similarity, finite-difference and Darcy model [7] solutions are presented. It is seen that both the local similarity method and Darcy model overestimate the centerline temperature and velocity. As expected, the agreement between local similarity and Keller's Box methods of solution deteriorates when ξ increases. For example, for the centerline temperature, the error for the local similarity method is 6% at $\xi = 0.1$ and 185% at $\xi = 8$, and for the centerline velocity it is 3.6% at $\xi = 0.1$ and 110% at $\xi = 8$. For a maximum error of 15%, the value of the centerline temperature is found to be satisfactory for the $\xi \leqslant 1$ value, while the value of the centerline velocity is satisfactory for $\xi \leqslant 3.5$.

CONCLUSION

The rigorous numerical solutions for the natural convection flow from a heat point source in a non-

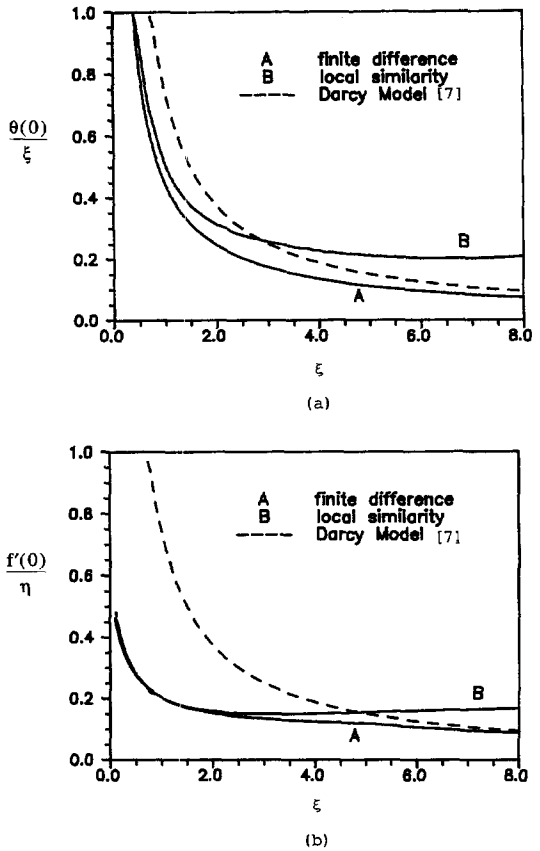

Fig. 10. The variation of dimensionless centerline temperature and velocity over a wide range of ξ with $Pr = 5.4$, $\Gamma = 1200$ and $\gamma = 0.15$.

Darcian porous medium are performed. A new parameter,

$$\xi = \frac{1}{(Da_x\, Ra_x^{1/2})}\left[= \left(\frac{2\pi k \alpha_0 \nu x^2}{K^2 g \beta Q}\right)^{1/2}\right]$$

characterizes the source strength (Q), the distance along the plate from the leading edge (x), the permeability (K) of the porous medium is introduced, and Darcy's law corresponds to the case of $\xi \to \infty$ with $\Gamma = 0$ and $\gamma = 0$. It is shown that the Darcy model overestimates both the centerline temperature and velocity. As the value of inertia effect parameter Γ is increased, the centerline velocity is decreased and the centerline temperature is increased, while, as the value of thermal dispersion coefficient γ is increased, both the centerline velocity and temperature are decreased. The numerical results also indicate that the local similarity method overpredicts both the centerline temperature and velocity. When compared with the Keller's Box method, for a largest error of 15%, the local similarity method is satisfactory only for $\xi \leqslant 1$.

Acknowledgement—Financial support was provided by the National Science Council of the Republic of China under contract NSC82-0401-E006-120.

REFERENCES

1. T. Fujii, Theory of the steady laminar natural convection above a horizontal line heat source and a point heat source, *Int. J. Heat Mass Transfer* **6,** 597–606 (1963).
2. J. A. Liburdy and G. M. Faeth, Theory of a steady laminar thermal plume along a vertical adiabatic wall, *Lett. Heat Mass Transfer* **2,** 407–418 (1975).
3. E. M. Sparrow, S. V. Patankar and R. M. Abdel-Wahed, Development of wall and free plumes above a heated vertical plate, *J. Heat Transfer* **100,** 184–190 (1978).
4. K. V. Rao, B. F. Armaly and T. S. Chen, Analysis of laminar mixed convective plumes along vertical adiabatic surfaces, *J. Heat Transfer* **106,** 552–557 (1984).
5. H. T. Lin and J. J. Chen, Mixed convection wall plumes, *Int. J. Heat Mass Transfer* **30,** 1721–1726 (1987).
6. R. A. Wooding, Convection in a saturated porous medium at large Rayleigh number or Peclet number, *J. Fluid Mech.* **15,** 527–544 (1963).
7. A. Bejan, *Convection Heat Transfer*, Chap. 10. Wiley, New York (1984).
8. F. C. Lai, Natural convection from a concentrated heat source in a saturated porous medium, *Int. Commun. Heat Mass Transfer* **17,** 791–800 (1990).
9. A. Bejan, Natural convection in an infinite porous medium with a concentrated heat source, *J. Fluid Mech.* **89,** Pt 1, 97–107 (1978).
10. C. E. Hickox and H. A. Watts, Steady thermal convection from a concentrated source in a porous medium, *J. Heat Transfer* **102,** 248–253 (1980).
11. C. E. Hickox, Thermal convection at low Rayleigh number from concentrated sources in porous medium, *J. Heat Transfer* **103,** 232–236 (1981).
12. N. Afzal and M. Y. Salam, Natural convection from point source embedded in Darcian porous medium, *Fluid Dynam. Res.* **6,** 175–184 (1990).
13. A. Nakayama, A similarity solution for free convection from a point heat source embedded in a non-Newtonian fluid-saturated porous medium, *J. Heat Transfer* **115,** 510–513 (1993).
14. M. Kumari, I. Pop and G. Nath, Darcian mixed convection plumes along vertical adiabatic surfaces in a saturated porous medium, *Therm. Fluid Dynam.* **22,** 173–178 (1988).
15. D. Poulikakos, On buoyancy induced heat and mass transfer from a concentrated source in an infinite porous medium, *Int. J. Heat Mass Transfer* **28,** 621–629 (1985).
16. S. E. Larson and D. Poulikakos, Double diffusion from a horizontal line source in an infinite porous medium, *Int. J. Heat Mass Transfer* **29,** 492–495 (1986).
17. F. C. Lai and Kulacki F. A., Coupled heat and mass transfer from a sphere buried in an infinite porous medium, *Int. J. Heat Mass Transfer* **33,** 209 (1990).
18. F. C. Lai, Coupled heat and mass transfer by natural convection from a horizontal line source in saturated porous medium, *Int. Commun. Heat Mass Transfer* **17,** 489–499 (1990).
19. D. B. Ingham, An exact solution for non-Darcy free convection from a horizontal line source of heat, *Therm. Fluid Dynam.* **22,** 125–127 (1988).
20. F. C. Lai, Non-Darcy natural convection from a line source of heat in saturated porous medium, *Int. Commun. Heat Mass Transfer* **18,** 445–457 (1991).
21. P. Cheng and T. M. Zheng, Mixed convection in the thermal plume above a horizontal line source of heat in a porous medium of infinite extent, *Proceedings of the 8th International Heat Transfer Conference*, San Francisco, CA, Vol. 5, pp. 2671–2675 (1986).
22. T. Cebeci and P. Bradshaw, *Physical and Computational Aspects of Convective Heat Transfer*, Chap. 13. Springer, New York (1984).
23. W. S. Yu, H. T. Lin and H. C. Shih, Rigorous numerical solutions and correlations for two-dimensional laminar

buoyant jets, *Int. J. Heat Mass Transfer* **35,** 1131–1141 (1992).
24. O. A. Plumb, The effect of thermal dispersion on heat transfer in packed bed boundary layers, *Proceedings of the 1st ASME/JSME Thermal Engineering Joint Conference*, Vol. 2, pp. 17–21. ASME, Tokyo (1983).
25. S. Ergun, Fluid flow through packed columns. *Chem. Engng Prog.* **48,** 89–94 (1952).